AUT Journal of Electrical Engineering

AUT J. Elec. Eng., 51(2) (2019) 123-130
DOI: 10.22060/eej.2019.14446.5229

Sea Surfaces Scattering by Multi-Order Small-Slope Approximation: a Monte-Carlo and Analytical Comparison

N. Radkani, B. Zakeri*

Department of Electrical and Computer Engineering, Babol Noshirvani University, Babol, Iran

ABSTRACT: L-band electromagnetic scattering from two-dimensional random rough sea surfaces are calculated by first- and second-order Small-Slope Approximation (SSA1, 2) methods. Both analytical and numerical computations are utilized to calculate incoherent normalized radar cross-section (NRCS) in mono- and bi-static cases. For evaluating inverse Fourier transform, inverse fast Fourier transform (IFFT) is performed to reduce computational burdens. For the SSA simulations, surface dimensions are large as all sea spectrum components are included. Considering the integration domain of the Analytical SSA (A-SSA), it requires huge computer memories especially at high frequencies and high wind speeds. In this regard, the numerical SSA (N-SSA) employs less memory, however, it requires more running time because of Monte-Carlo simulations. By applying tapered incident plane wave (TPW) to the N-SSA, dimensions are reduced to enhance computational efficiency in comparison with the A-SSA. As a result, the N-SSA with the TPW is applicable to high wind speeds, where the A-SSA may be limited. To validate the SSA, Results are compared with those from the method of moments (MoMs) in VV polarization. The results of different methods show good agreements at low wind speeds and incident angles less than 60 degrees. At high wind speeds, there are some differences between the SSA1 and the SSA2 recommending on the SSA2 to use, due to the higher order of accuracy.

Review History:
Received: 2018-05-16
Revised: 2019-01-23
Accepted: 2019-07-09
Available Online: 2019-12-01

Keywords:
Electromagnetic scattering
normalized radar cross-section
sea surface
small-slope approximation

I. INTRODUCTION

The problem of electromagnetic (EM) scattering from a sea surface has practical interest. The sea surface roughness strongly influenced by local winds, scatter the electromagnetic waves. The sea frequency spectrum, which used in the scattering model, is the function of wind speed and direction above sea level, inverse wave age and other marine parameters [1]. Accordingly, the scattering models of sea surfaces can be used for physical interpretations of marine phenomena and also retrieving the marine parameters such as wave heights and local winds.

The methods for investigating the scattering from random rough surfaces primarily are two kinds: exact numerical and approximate analytical methods. The most common numerical methods are method of moments (MoM) [2], finite element method (FEM) [3], finite-difference time-domain (FDTD) [4], extended boundary condition method (EBCM) [5] and boundary perturbation method [6,7]. The numerical methods are characterized by high computational precision. However, the computation burdens and memory requirements, which depend on the frequency and scatterer size, limit the application of numerical techniques. Many efforts accomplished to handle the significant memory requirements and accelerate the numerical models. However, these models may still not be suitable to solve rough surface scattering problems, particularly for the electrically large sea surface.

The widely used approximate analytical methods for rough surface scattering are mainly Kirchhoff approximation (KA) [8,9], small perturbation method (SPM) [8-10], advanced integral equation model (AIEM) [11], two-scale model (TSM) [12] and small-slope approximation (SSA) [13-19]. In the methods, the sea surface roughness is divided into two scales: small-scale roughness (capillary waves) and large-scale (gravity waves) roughness. The SPM, which is often referred as a low-frequency approach, is limited to surfaces with rather small height variations (small-scale roughness) and relatively small slopes. The KA, which is referred as a high-frequency method, requires that every point on the rough surface have a large radius of curvature relative to the wavelength (large-scale roughness). The TSM combines two approaches to calculate the scattering problem of sea surfaces, which hold for the large-scale rough surface and the small-scale one, respectively. The classical TSM combines the SPM and the KA. The existence of a gap between validity regions of the SPM and KA makes the TSM model inaccurate for conFigurations that are beyond the validity regions. Among these methods, the SSA is a unifying theory, which is appropriate for microwave scattering from random rough surfaces in small roughness slope compared to the grazing angle and the scattering grazing angle at many wave bands. The SSA bridges and

*Corresponding author's email: zakeri@nit.ac.ir

extends the SPM and KA and it is developed in two orders of accuracy; first-order (SSA1) and second-order (SSA2). Due to the high precision of the SSA, it has been widely applied to the calculation of sea surface scattering and Doppler spectrum for linear and nonlinear sea surfaces [17]. The aim of recent studies is mainly accelerating the method and reducing the computational burden [18,19].

Computations in the SSA can be performed in two ways: numerical and analytical. In the numerical SSA (N-SSA), many random rough surfaces are generated using the surface frequency spectrum. The scattering amplitude of these surfaces is calculated separately and then the ensemble average of the scattering amplitudes is taken using Monte-Carlo technique to find the normalized radar cross-section (NRCS). In the analytical SSA (A-SSA), the ensemble average of scattering amplitude's equation is used directly for calculating the NRCS. This method requires the correlation function and the frequency spectrum of the rough surfaces. In the sea surface scattering problem, the dimensions of the surface must satisfy a condition that is directly proportional to the second power of wind speed. By increasing the wind speed, the surface dimensions, accordingly, the required memory and the time for computations are increased. Consequently, at high wind speeds, there are limitations in both the memory requirements and the run time of the SSA computations.

In this paper, the SSA1 and the SSA2 are used to calculate the incoherent scattering of electromagnetic waves from two dimensional (2-D) random rough sea surfaces based on both the analytical and numerical computations. Results show which method is efficient. The simulations are performed in L-band frequency with the application of Phased Array L-Band Synthetic Aperture Radar (PALSAR) on the Advanced Land Observing Satellite (ALOS) and Global navigation satellite system (GNSS) reflectometry in mono- and bi-static conFigurations, respectively. In the A-SSA simulations, the surface dimensions are large enough for including all components of the sea spectrum. In the N-SSA, by applying the tapered incident wave, we perform the simulations for two different sizes of surface sides; a size that satisfies the related condition, and a size that is smaller four times. We compare the methods together about their accuracy, run time and required memory. The methods are validated by comparison with the MoM in VV polarization.

This paper is organized as follows. In section II, the SSA formulation based on both analytical and numerical computations for NRCS calculation is described. The simulations of the mono- and the bi-static scattering of the sea surfaces based on equations of section II and the acquired results are presented in section III. Finally, section IV concludes the paper.

II. ROUGH SURFACE SCATTERING FORMULATION

In this section, we evaluate a scattering amplitude based on the SSA2. The geometrical conFiguration adopted to solve the electromagnetic scattering from the 2-D rough sea surface is shown in Fig. 1, where θ_i and θ_s are incident and scattering angles, respectively, and φ_i and φ_s are incident and scattering azimuth angles, respectively. The rough surface sides in x and y directions are L_x and L_y, respectively.

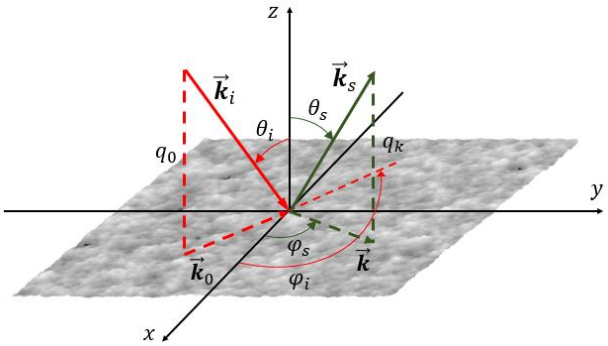

Fig. 1. Geometry configuration for scattering from rough sea surface.

The upper medium is air described with wavenumber of free space $K_0 = 2\pi/\lambda$ (λ is microwave wavelength). The lower medium is described by a homogeneous complex relative permittivity ε_r and a complex wavenumber $K = \sqrt{\varepsilon_r} K_0$. Incident wave vector is defined by $\dot{k}_i = \dot{k}_0 - q_0 \hat{z}$ where $\dot{k}_0$ and $-q_0$ are horizontal and vertical projections of the incident wave vector, respectively and are related to the incident angle θ_i by

$$k_0 = K_0 \sin\theta_i, q_0 = K_0 \cos\theta_i \tag{1}$$

Scattered wave vector is expressed as $\dot{k}_s = \dot{k} + q_k \hat{z}$ where $\vec{k}$ and q_k are horizontal and vertical projections of the scattered wave vector, respectively and are related to the scattering angle θ_s by

$$k = K_0 \sin\theta_s, \; q_k = K_0 \cos\theta_s \tag{2}$$

The scattering amplitude in the SSA2 has the following form [15]:

$$\left(S_2\right)_{\alpha\alpha_0}\left(\vec{k},\vec{k}_0\right) = \frac{2\left(q_k q_0\right)^{1/2}}{Q} \times \int \exp\left[-i\left(\vec{k}-\vec{k}_0\right)\vec{r} + iQh\left(\vec{r}\right)\right] \times \left(B_{\alpha\alpha_0}\left(\vec{k},\vec{k}_0\right) - \frac{i}{4}\int M_{\alpha\alpha_0}\left(\vec{k},\vec{k}_0;\vec{\xi}\right)\hat{h}\left(\vec{\xi}\right)\exp\left(i\vec{\xi}\vec{r}\right)d\vec{\xi}\right) \times \frac{d\vec{r}}{(2\pi)^2} \tag{3}$$

$$M_{\alpha\alpha_0}\left(\dot{k},\dot{k}_0;\dot{\xi}\right) = \left(B_2\right)_{\alpha\alpha_0}\left(\dot{k},\dot{k}_0;\dot{k}-\dot{\xi}\right) + \left(B_2\right)_{\alpha\alpha_0}\left(\dot{k},\dot{k}_0;\dot{k}_0+\dot{\xi}\right) + 2QB_{\alpha\alpha_0}\left(\dot{k},\dot{k}_0\right) \tag{4}$$

where $Q = q_k + q_0$ and $\vec{r} = (x, y)$ is position vector. The subscripts α_0 and α are incident and scattered wave polarizations respectively. $h(\vec{r})$ is surface elevation and $h(\xi)$ is the Fourier transform of $h(\vec{r})$:

$$\hat{h}(\vec{\xi}) = \int h(\vec{r})\exp\left(-i\vec{\xi}\vec{r}\right)\frac{d\vec{r}}{(2\pi)^2} \tag{5}$$

The first- and second-order Bragg kernels B and B_2, respectively, are 2 × 2 matrices and they depend on the

scattering geometry and dielectric constant of the medium [15]. The second term in equation (3) is an integral over 2-D spectral domains that can be calculated by an inverse Fourier transform. The integral over $\vec{r}$ is calculated numerically over 2-D spatial domains. Due to the random characteristics of the rough sea surfaces, their profiles are described by stochastic processes and therefore, the mono- and bi-static NRCSs are calculated by averaging. The incoherent NRCS is calculated as follows:

$$\sigma_{\alpha\alpha_0} = 4\pi q_0 q_k \left[\left\langle \left| S_{\alpha\alpha_0} \right|^2 \right\rangle - \left| \left\langle S_{\alpha\alpha_0} \right\rangle \right|^2 \right] \quad (6)$$

where $\langle \ldots \rangle$ denotes the average over the total number of scattering amplitudes. Two computational methods for computing the NRCS can be used in the SSA method: numerical and analytical computations. We describe these methods in the next two sections.

A) N-SSA

In order to the numerical computations of the NRCS in the SSA, many realizations of rough surfaces are generated using the surface spectrum to realize the Monte-Carlo simulation. The scattering amplitude of each surface is calculated using the equation (3). Then, the incoherent NRCS is calculated by the ensemble averaging of the scattering amplitudes based on the equation (6). In order to avoid artificial edge diffraction resulting from the finite dimensions of the simulated rough surface, the tapered plane wave can be applied to the scattering amplitude formulation rather than the generally used plane wave. The tapering function $T\left(\vec{r}, h\left(\vec{r}\right)\right)$has the following form [20]:

$$T\left(\vec{r}, h\left(\vec{r}\right)\right) = \exp\left[-i\left(\vec{k}_0.\vec{r} - q_0 h\left(\vec{r}\right)\right) w \right] \exp\left(-t_x - t_y\right) \quad (7)$$

$$w = \left(1 / K_0^{\,2}\right)\left[\left(2t_x - 1\right) / \left(g^2 \cos^2\theta_i\right) + \left(2t_y - 1\right) / g^2 \right] \quad (8.a)$$

$$t_x = \left(x\cos\theta_i \cos\varphi_i + y\cos\theta_i \sin\varphi_i + h\left(\vec{r}\right)\sin\theta_i \right)^2 \quad (8.b)$$

$$t_y = \left(-x\sin\varphi_i + y\cos\varphi_i\right)^2 / g^2 \quad (8.c)$$

where g is tapering parameter. By introducing the tapering function into the integral term of equation (3), the scattering amplitude can be modified as [17]:

$$\begin{aligned} &\left(S_2\right)_{\alpha\alpha_0}\left(\vec{k},\vec{k}_0\right) = \frac{2\left(q_k q_0\right)^{1/2}}{Q\sqrt{P_{inc}}} \times \\ &\int \exp\left[-i\left(\vec{k} - \vec{k}_0\right)\vec{r} + iQh\left(\vec{r}\right) \right] \times \\ &\left(B_{\alpha\alpha_0}\left(\vec{k},\vec{k}_0\right) - \frac{i}{4}\int M_{\alpha\alpha_0}\left(\vec{k},\vec{k}_0;\vec{\xi}\right)\hat{h}\left(\vec{\xi}\right)\exp\left(i\vec{\xi}\vec{r}\right)d\vec{\xi} \right) \times \\ &T\left(\vec{r}, h\left(\vec{r}\right)\right) \times \frac{d\vec{r}}{(2\pi)^2} \end{aligned} \quad (9)$$

where P_{inc} is the incident wave power received by the rough surface. In equation (9), the second term can be evaluated using an inverse Fourier transform. The integral over $\vec{r}$ is calculated numerically over spatial domains with $x \in [-L_x/2, L_x/2]$ and $y \in [-L_y/2, L_y/2]$.

B) A-SSA

In order to the analytical computations of NRCS in the SSA, the correlation function and the frequency spectrum of the rough surface are required instead of the surface elevation. By averaging the scattering amplitude formula using equation (6), the incoherent NRCS is calculated as follows [13]:

$$\sigma_{\alpha\alpha_0}\left(\vec{k},\vec{k}_0\right) = \left(\frac{2q_k q_0}{Q\sqrt{\pi}}\right)^2 \times \int R_{\alpha\alpha_0}\left(\vec{k},\vec{k}_0;\vec{r}\right)\exp\left[-i\left(\vec{k} - \vec{k}_0\right)\right] d\vec{r} \quad (10)$$

$$\begin{aligned} &R_{\alpha\alpha_0}\left(\vec{k},\vec{k}_0;\vec{r}\right) = -\exp\left[-Q^2 C(0) \right] \times \\ &\left| B_{\alpha\alpha_0}\left(\vec{k},\vec{k}_0\right) - F_{\alpha\alpha_0}\left(\vec{k},\vec{k}_0;0\right) \right|^2 + \\ &\exp\left[-Q^2\left(C(0) - C(\vec{r})\right) \right] \times \\ &G_{\alpha\alpha_0}\left(\vec{k},\vec{k}_0;\vec{r}\right) + \left(\begin{array}{l} B_{\alpha\alpha_0}\left(\vec{k},\vec{k}_0\right) - \\ F_{\alpha\alpha_0}\left(\vec{k},\vec{k}_0;0\right) + \\ F_{\alpha\alpha_0}\left(\vec{k},\vec{k}_0;\vec{r}\right) \end{array} \right) \times \left(\begin{array}{l} B_{\alpha\alpha_0}\left(\vec{k},\vec{k}_0\right) - \\ F_{\alpha\alpha_0}\left(\vec{k},\vec{k}_0;0\right) + \\ F_{\alpha\alpha_0}\left(\vec{k},\vec{k}_0;\vec{r}\right) \end{array} \right)^* \end{aligned} \quad (11)$$

where $\vec{r} = \vec{r}_2 - \vec{r}_1$ is defined as the difference between two horizontal position vectors $\vec{r}_1$and $\vec{r}_2$. Consequently, for a surface with dimensions $L_x \times L_y$, integration over$\vec{r}$ is performed numerically on a spatial domain with $x \in [-L_x, L_x]$ and $y \in [-L_y, L_y]$ (the integral domain is 4 times the integral domain of N-SSA).$C(\vec{r})$ is correlation function of rough surface and is calculated by the inverse Fourier transform of directional spectrum of surface$W(\vec{k})$:

$$C\left(\vec{r}\right) = \int W\left(\vec{\xi}\right)\exp\left(i\vec{\xi}\vec{r}\right)d\vec{\xi} \quad (12)$$

$F_{\alpha\alpha_0}\left(\vec{k},\vec{k}_0;\vec{r}\right)$and $G_{\alpha\alpha_0}\left(\vec{k},\vec{k}_0;\vec{r}\right)$are calculated by the inverse Fourier transformation as follows:

$$F_{\alpha\alpha_0}\left(\vec{k},\vec{k}_0;\vec{r}\right) = -\frac{Q}{4}\int M_{\alpha\alpha_0}\left(\vec{k},\vec{k}_0;\vec{\xi}\right)W\left(\vec{\xi}\right)\exp\left(i\vec{\xi}\vec{r}\right)d\vec{\xi} \quad (13)$$

$$G_{\alpha\alpha_0}\left(\vec{k},\vec{k}_0;\vec{r}\right) = \frac{1}{16}\int \left| M_{\alpha\alpha_0}\left(\vec{k},\vec{k}_0;\vec{\xi}\right)\right|^2 W\left(\vec{\xi}\right)\exp\left(i\vec{\xi}\vec{r}\right)d\vec{\xi} \quad (14)$$

Setting $M_{\alpha\alpha_0} = 0$in both the N-SSA and the A-SSA equations, one obtains the SSA1.

III. SIMULATIONS AND RESULTS

In the sea surface scattering problem, the radar and radiometer pixels from satellites are large and the pixels can be more than hundreds of thousands of square wavelengths. However, in simulations, the surface size is finite and cannot

be as large as radar pixel. On the other hand, the surface cannot be small and needs to be large enough to include the largest waves of the sea surface. In order to correctly represent the surface gravity waves in the sea surface scattering problem, the surface sides L_x and L_y need to satisfy the condition as follows [21]:

$$L_x, L_y > 20u_{10}^2 / (g.\Omega^2) \tag{15}$$

where u_{10} is wind speed at 10 meters above the mean sea level, g is gravity acceleration and taken as 9.81 m/s^2, and Ω is the inverse wave age taken as 0.84 for fully developed seas. We set the surface length $L_x = L_y = L$ and the sampling interval $\Delta x = \Delta y$. A finite surface size means that the sea spectrum is truncated between k_l and k_u, where k_l is inversely proportional to the surface size while k_u is inversely proportional to the discretizing sampling [22]:

$$k_l = \frac{2\pi}{L}\ ,\ k_u = \frac{\pi}{\Delta x} \tag{16}$$

If surface sides do not satisfy the condition (15), then k_l get larger and this means that the gravity waves of the sea surface are significantly truncated.

Both the NRCS formulations with the analytical and the numerical methods involve two-fold 2-D integrals (one over the sea wavenumber ξ and one over the radial distance r). However, if the inverse Fourier transforms are first evaluated using inverse fast Fourier transform (IFFT) algorithm before proceeding to the spatial integration, the spatial and spectral integrations become decoupled, and only two 2-D integrations are necessary. Consequently, the computation time reduced significantly. According to standard FFT rules, the number of samples is chosen as the power of two to be able to use an IFFT. When using an FFT algorithm, the spectral discretization is determined by the spatial discretization according to standard FFT rules.

For NRCS simulations, the frequency is 1.27 GHz (L-band) and the relative permittivity of the sea water is set $\varepsilon_r = 75 + i\,61$. To solve the EM problem which considers a very conducting medium, ideally, the sampling interval Δx is rather $\lambda/10$. We set the sampling interval $\Delta x = \lambda/10$. For backscattering calculations, the angles are set as $\theta_s = \theta_i$, $\varphi_s = \varphi_i + 180^\circ$. The incident wave slants at $0^\circ < \theta_i \leq 80^\circ$ with angle step 5˚. For bi-static scattering calculations, the incident and scattering angles are set as $\theta_i = 30^\circ, 60^\circ$, $-80^\circ \leq \theta_s \leq 80^\circ$, $\varphi_i = \varphi_s$.

From the Bragg scattering theory, the spectral component of the sea spectrum that contributes to the backscattering is at $k_B = 2\,K_0 \sin(\theta_i)$. We use Elfouhaily directional spectrum [1] which is developed for the sea surface. In Fig. 2, a log–log scale of the isotropic part of the Elfouhaily spectrum for a wind speed u_{10} = 3 m/s, the microwave wavenumber K_0, Bragg wavenumber k_B for $\theta_i = 1^\circ, 80^\circ$, k_l for surface length and k_u for sampling interval used in the SSA simulations are shown. As seen in Fig. 3, the significant part of the spectrum,

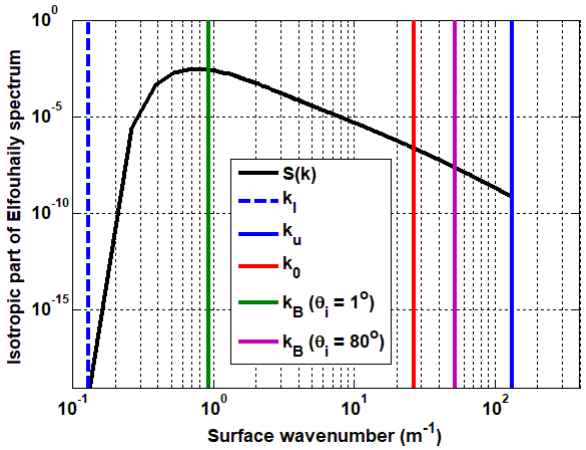

Fig. 2. isotropic part of surface spectrum for a wind speed 3 m/s.

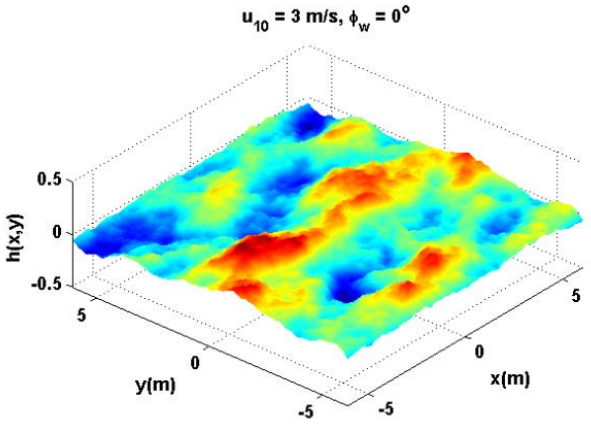

Fig. 3. One realization of rough sea surface generated by Elfouhaily spectrum

the microwave wavenumber and Bragg wavenumber fall between the lower limit and the upper limit of the spectral components.

For the numerical computations of the SSA, the surface elevation is required; therefore, a number of 2-D random rough surfaces must be generated by sea spectrum. The numerical details of 2-D rough surface generation can be found in [5]. One realization of rough sea surface generated by Elfouhaily spectrum for a wind speed 3 m/s is shown in Fig. 3.

Then, Monte-Carlo simulations of the scattering from many realizations need to be carried out and convergence of realizations need to be shown. Fig. 4 shows the convergence of the backscattering NRCSs as a function of the realizations of simulation for three incident angles $\theta_i = 1^\circ, 40^\circ, 80^\circ$. It can be seen at all incident angles, the backscattering NRCSs converge about 30 realizations. Therefore, the use of 50 realizations confidently yields the convergence of backscattering NRCSs for the N-SSA simulations.

For a wind speed of u_{10} = 3 m/s and a wind direction relative to radar incidence $\varphi_w = 0$ (upwind direction), the sea surface is made of 2048 × 2048 samples, so that the surface sides have a length $L \cong 48.38$ m. For a wind speed of $u_{10} = 5$

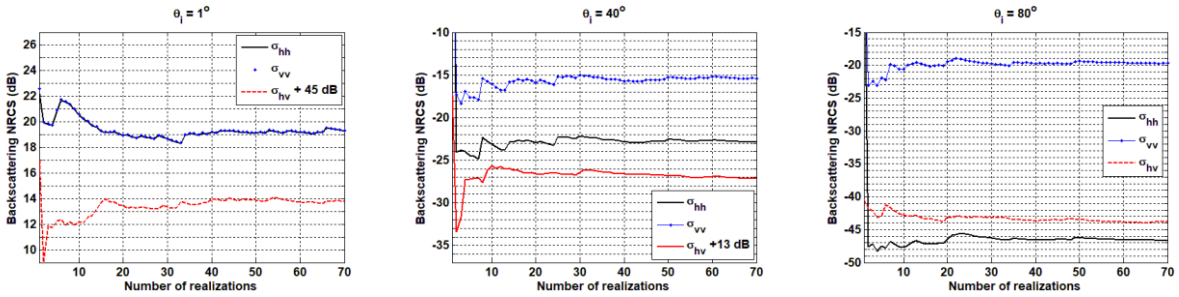

(a) (b) (c)

Fig. 4. Convergence of backscattering NRCSs in dB as a function of realizations for three incident angles; (a) $\theta_i = 1^\circ$, (b) $\theta_i = 40^\circ$, (c) $\theta_i = 80^\circ$.

m/s and upwind direction, the sea surface is made of 4096 × 4096 samples, so that the surface sides have a length $L \cong 96.75$ m. In the numerical computations, the size of the integration domain is equal to the sea surface size. The tapering parameter g should satisfy the condition $L/6 \le g \le L/4$ and is chosen to be $L/5$. Each NRCS is calculated by averaging over 50 realizations of sea surfaces.

In the analytical computations, we use Elfouhaily spectrum again. Considering to the integration domain in the A-SSA method, for the wind speed 3 m/s, the size of the integral domain is 96.75 × 96.75 m^2, sampled with 4096 × 4096 samples and for the wind speed 5 m/s, the size of the integral domain is 193.5 × 193.5 m^2, sampled with 8192 × 8192 samples. Therefore, the A-SSA includes all of the components of the spectrum. Fig. 5 shows the comparison of the monostatic incoherent NRCS in VV polarization versus incident angle evaluated by the SSA1 and the SSA2 from both the numerical and the analytical computations with the MoM from [2]. The results show good agreements for low and moderate angles ($\theta_i \le 60^\circ$) that are interesting in remote sensing applications. However, for large incident angles, the SSA methods, do not predict the NRCS correctly, because the accuracy of the spectral discretization is not enough for large angles. Therefore, for the NRCS prediction at large angles, the dimensions of the surface must be very larger than the related condition. For example, we plot the monostatic NRCS calculated by the A-SSA2 for the integral domain 483.78 × 483.78 m^2 sampled with 16384 × 16384 samples (black stars) in Fig. 5. The results are closed to the MoM results rather than the result of the A-SSA2 with the integral domain 96.75 × 96.75 m^2 (pink circles). However, the memory requirement is increased significantly.

In the N-SSA, when the tapered incident wave is used, the surface length can set smaller. For example, at the wind speed 3 m/s, surface length L must be 48.38 m or larger. However, if we use the tapered incident wave, we can set $L \cong 12.09$ m. Fig. 6a shows the comparisons of the monostatic NRCSs (HH, VV and HV polarizations) versus incident angle calculated by the N-SSA2 for these two surface lengths. The similar comparisons for the wind speed 5 m/s are seen in Fig. 6b. The results show good agreements. Consequently, in later simulations, we use the surfaces with the reduced sizes $L \cong 12.09$ m and $L \cong 24.19$ m for the numerical computations at

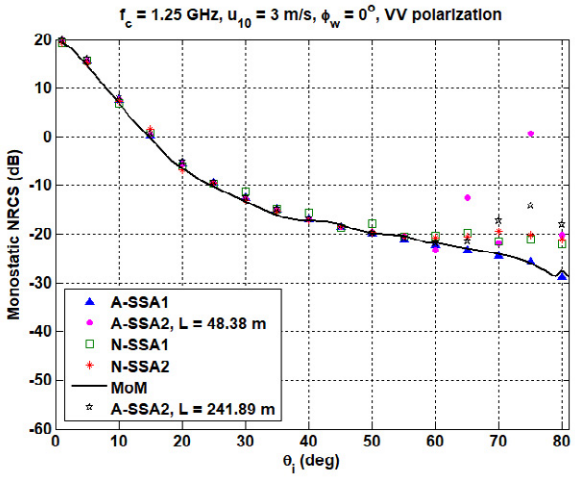

Fig. 5. Monostatic NRCS in VV polarization: Comparison of SSA1 from both numerical and analytical computations, SSA2 from both numerical and analytical computations and MoM from [2].

the wind speeds 3 and 5 m/s, respectively.

Fig. 7 shows the comparison of the mono-static incoherent NRCS of the sea surface at the wind speed 3 m/s versus incident angle calculated by various SSA methods. The co-polar results in Fig. 7.a and b show good agreements between the A-SSA1, the N-SSA1, the A-SSA2 and the N-SSA2 methods, except for very large incident angles which the A-SSA2 shows discrepancy with other results. As said before, this problem is solved by selecting the very larger surfaces. The cross-polar results in Fig. 7.c show good agreements between the A-SSA2 and the N-SSA2 method. The HV and VH polarizations are same in backscattering conFiguration and the cross-polar backscattering cannot be calculated by the SSA1. The similar comparisons for the wind speed 5 m/s are seen in Fig. 8. At the wind speed 5 m/s, the results show fewer agreements than those for wind speed 3 m/s. it is deduced that with increasing wind speed and consequently surface roughness, the accuracy of first-order solutions is decreased. Therefore, at moderate and high wind speeds, the SSA2 gives the more accurate results and must be utilized for the scattering calculations.

We compare the methods in bi-static case for two different incident angles. The comparisons of the bi-static incoherent NRCS of the sea surface versus scattering angle calculated by

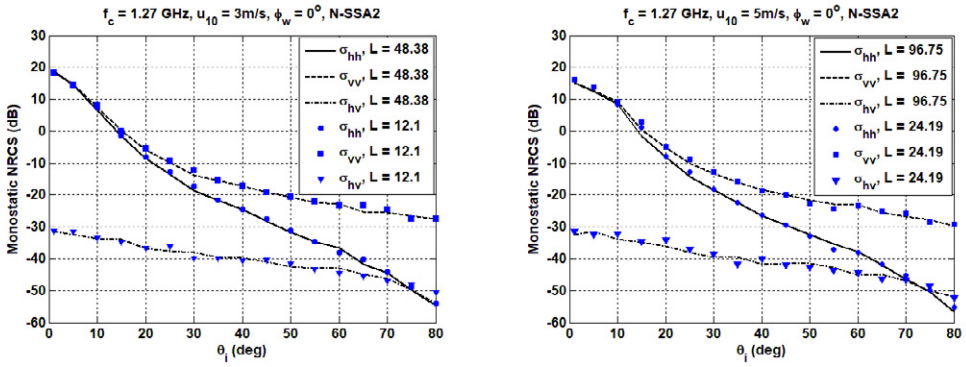

(a) (b)

Fig. 6. Comparison of monostatic NRCSs calculated by SSA2 from numerical computation: (a) at a wind speed 3m/s for L = 48.38 m with L = 12.1 m. (b) at a wind speed 5m/s for L = 96.75 m with L = 24.19 m. NRCSs are averaged over 50 surface realizations.

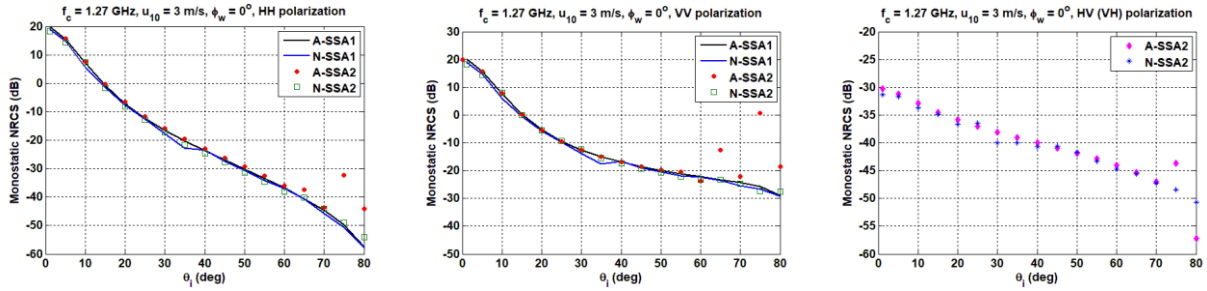

(a) (b) (c)

Fig. 7. Comparison of monostatic NRCS of sea surface at a wind speed 3 m/s calculated by 1- and 2-order SSA from both numerical and analytical computations. (a) HH polarization, (b) VV polarization, (c) HV or VH polarization.

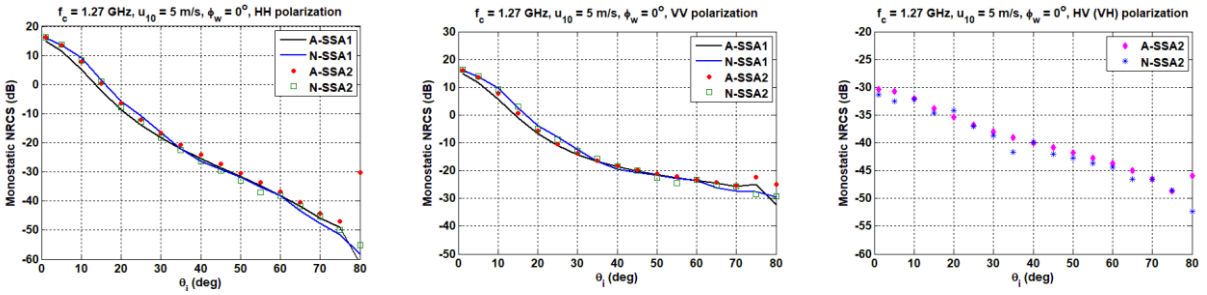

(a) (b) (c)

Fig. 8. Comparison of monostatic NRCS of sea surface at a wind speed 5 m/s calculated by 1- and 2-order SSA from both numerical and analytical computations. (a) HH polarization, (b) VV polarization, (c) HV or VH polarization.

various SSA methods at the wind speed 3 m/s, for incident angle θ_i = 30° are shown in Fig. 9. The co-polar results in Fig. 9.a and b show good agreements between the A-SSA1, the N-SSA1, the A-SSA2 and the N-SSA2 methods at the different scattering angles. The cross-polar results in Fig. 9.c and d show good agreements between the A-SSA2 and the N-SSA2 methods. The cross-polar scattering in the plane of incidence cannot be calculated by the SSA1. The similar comparisons for the incident angle θ_i = 60° are seen in Fig. 10. In this case, the methods also have good agreements.

All simulations are performed using MATLAB with an Intel(R) Core(TM) i7-4790K CPU at 4.00GHz frequency and 32-GB RAM computer. At the wind speed 3 m/s, the calculation time and memory for the all mono-static simulations are estimated by CPU and are available in Table I. Considering to the accuracy and the running time of first- and second-order methods, we can use the SSA1 for calculating the co-polar components of scattering at low wind speeds. The A-SSA in comparison with the N-SSA is faster, however, needs further memory, because, for the same problem, the integration domain of the A-SSA should be 4 times the integration domain of the N-SSA. Therefore, if a computer with huge memory is available, the A-SSA can be employed. Otherwise, the N-SSA must be used in the longer time (due to Monte-Carlo simulations) to obtain results. In the numerical method, if the tapered plane wave is used, then the

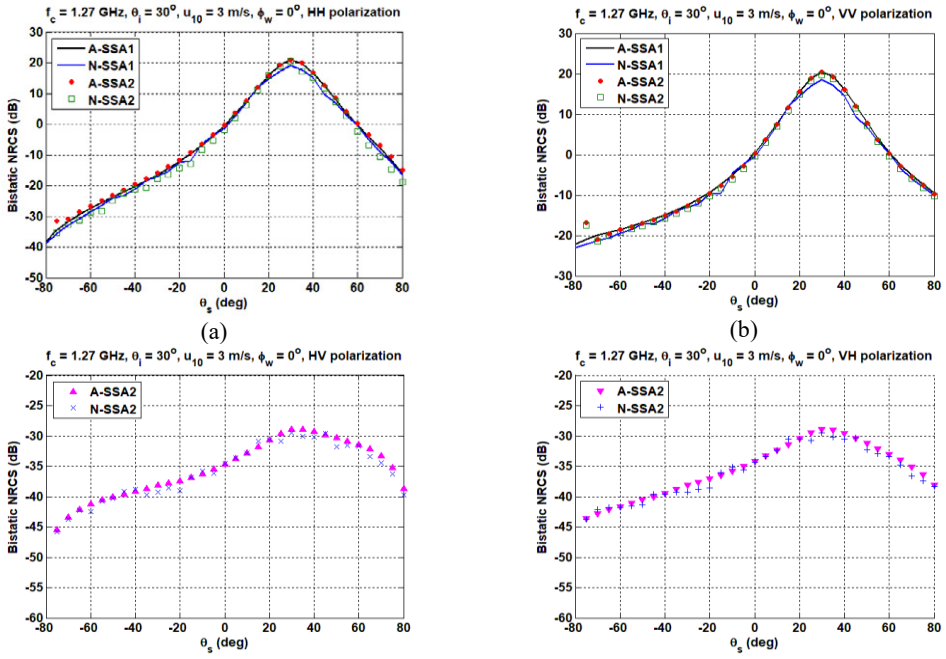

Fig. 9. Comparison of bistatic NRCS of sea surface calculated by 1- and 2-order SSA from both numerical and analytical computations for incident angle of 30˚. (a) HH, (b) VV, (c) HV and (d) VH polarization.

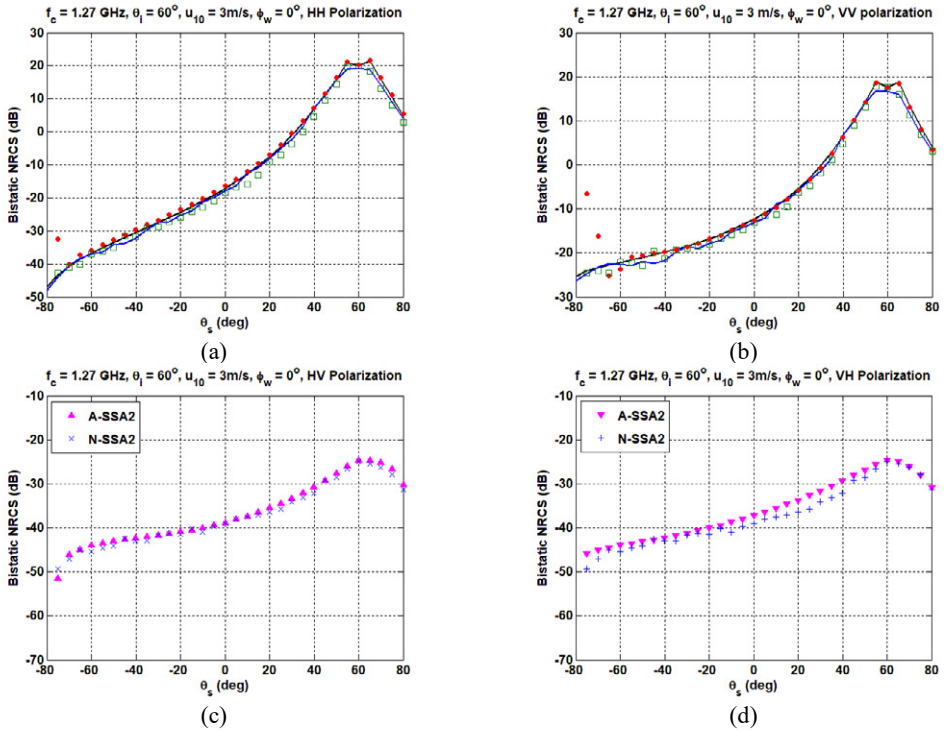

Fig. 10. Comparison of bistatic NRCS of sea surface calculated by 1- and 2-order SSA from both numerical and analytical computations for incident angle of 60˚. (a) HH, (b) VV, (c) HV and (d) VH polarization.

dimensions of the surface can be set smaller. Consequently, both the running time and memory consumption decreased significantly. Therefore, this method can be used even for high wind speeds where the analytical method and the numerical method without tapering have poor computational efficiency.

IV. Conclusion

The SSA is a high precision method for the calculation of rough surface scattering problems. In this paper, using both the analytical and the numerical computation of the SSA in first- and second-order, the electromagnetic scattering from

Table I. Calculation times and memories for analytical and numerical computation of 1- and 2-order SSA at a wind speed 3 m/s.

Method	L (m)	Integration domain (m^2)	Time (sec)	Memory (MB)
A-SSA1	48.378	96.75 × 96.75	37	1296
N-SSA1	48.378	48.38 × 48.38	609	378
N-SSA1	12.0945	12.09 × 12.09	39	24
A-SSA2	48.378	96.75 × 96.75	290	4992
N-SSA2	48.378	48.38 × 48.38	3015	802
N-SSA2	12.0945	12.09 × 12.09	176	61

the rough sea surface has been calculated in L-band frequency at two wind speeds 3 and 5 m/s. The accuracy of the methods is compared with the MoM at the wind speed 3 m/s for VV polarization and the results show good agreements for $\theta_i \leq 60°$. According to the results, the first-order methods can be trusted for calculating the co-polar components of scattering at low wind speeds. However, the SSA2 should be employed at moderate and high wind speeds. The A-SSA in comparison with the N-SSA has a smaller running time but needs the larger memory considering to the integration domain. Besides, at high wind speeds, the dimensions of the integration domain and the number of samples are very large and the computations require the huge memory and running time. Therefore, it may that the available memory of computer do not be enough for the SSA computations. By applying the tapered incident plane wave to the N-SSA, the surface dimensions can set smaller so that the dimensions of surface do not satisfy the related condition, consequently, the computational time and required memory are decreased significantly. Therefore, the N-SSA with tapering is the most suitable method about computational efficiency and can solve the problem at high wind speeds where the analytical method and the numerical method without tapering is not able to solve them.

V. REFERENCES

[1] T. Elfouhaily, B. Chapron, K. Katsaros, D. Vandemark, A unified directional spectrum for long and short wind-driven waves, J. Geophys. Res., 102(C7) (1997).

[2] D. Miret, G. Soriano, M. Saillard, Rigorous Simulations of Microwave Scattering from Finite Conductivity Two-Dimensional Sea Surfaces at Low Grazing Angles, IEEE Trans. Geosci. Remote Sens., 52(6) (2014).

[3] O. Ozgun, M. Kuzuoglu, Monte Carlo-Based Characteristic Basis Finite-Element Method (MC-CBFEM) for Numerical Analysis of Scattering from Objects On/Above Rough Sea Surfaces, IEEE Trans. Geosci. Remote Sens., 50(3) (2012).

[4] F.D. Hastings, J.B. Schneider, S.L. Broschat, A Monte-Carlo FDTD Technique for Rough Surface Scattering, IEEE Trans. Antennas Propag., 43(11) (1995).

[5] X. Duan, M. Moghaddam, 3-D Vector Electromagnetic Scattering from Arbitrary Random Rough Surfaces Using Stabilized Extended Boundary Condition Method for Remote Sensing of Soil Moisture, IEEE Trans. Geosci. Remote Sens., 50(1) (2012).

[6] D.P. Nicholls, A rapid boundary perturbation algorithm for scattering by families of rough surfaces, J. Comput. Phys., 228(9) (2009).

[7] J.Y. Liu, C.F. Huang, P.C. Hsueh, Acoustic plane-wave scattering from a rough surface over a random fluid medium, Ocean Eng. , 29(8) (2002).

[8] L. Tsang, J.A. Kong, K.H. Ding, Scattering of Electromagnetic Waves: Theories and Applications, Wiley, Hoboken, NJ, USA, 2000.

[9] L. Tsang, J.A. Kong, Scattering of Electromagnetic Waves: Advanced Topics, Wiley, Hoboken, NJ, USA, 2001.

[10] M.R. Mousavi, M. Karimi, A. Jamshidi, Probability distribution of acoustic scattering from slightly rough sea surface, Ocean Eng., 112(15) (2016).

[11] K.L. Chen, K.S. Chen, Z.L. Li, Y. Liu, Extension and Validation of an Advanced Integral Equation Model for Bistatic Scattering from Rough Surfaces, Progress in Electromagnetics Research, 152 (2015).

[12] G. Soriano, C.A. Guérin, A Cutoff Invariant Two-Scale Model in Electromagnetic Scattering From Sea Surfaces, IEEE Geosci. Remote Sens. Lett., 5(2) (2008).

[13] A.G. Voronovich, Small-slope approximation for electromagnetic wave scattering at a rough interface of two dielectric half-spaces, Waves in Random Media, 4(3) (1994).

[14] A.G. Voronovich, Wave Scattering from Rough Surfaces, Springer, Berlin, Germany, 1994.

[15] A.G. Voronovich, V.U. Zavorotny, Theoretical model for scattering of radar signals in Ku - and C-bands from a rough sea surface with breaking waves, Waves in Random Media, 11(3) (2001).

[16] A.G. Voronovich, V.U. Zavorotny, Full-Polarization Modeling of Monostatic and Bistatic Radar Scattering From a Rough Sea Surface, IEEE Trans. Antennas Propag., 62(3) (2014).

[17] X. Li, X. Xu, Scattering and Doppler Spectral Analysis for Two-Dimensional Linear and Nonlinear Sea Surfaces, IEEE Trans. Geosci. Remote Sens., 49(2) (2011).

[18] W. Jiang, M. Zhang, Y. Zhao, D. Nie, EM scattering calculation of large sea surface with SSA method at S, X, Ku, and K bands, Waves in Random and Complex Media, 27(1) (2016).

[19] J. Li, M. Zhang, P. Wei, W. Jiang, An Improvement on SSA Method for EM Scattering From Electrically Large Rough Sea Surface, IEEE Geosci. Remote Sens. Lett., 13(8) (2016).

[20] L. Tsang, J.A. Kong, K.H. Ding, C.O. Ao, Scattering of Electromagnetic Waves: Numerical Simulations, Wiley, New York, 2001.

[21] N. Pinel, C. Bourlier, Electromagnetic Wave Scattering from Random Rough Surfaces: Asymptotic models, Wiley, Hoboken, NJ, USA, 2013.

[22] L. Tsang, T.H. Liao, S. Tan, H. Huang, T. Qiao, K.H. Ding, Rough Surface and Volume Scattering of Soil Surfaces, Ocean Surfaces, Snow, and Vegetation Based on Numerical Maxwell Model of 3-D Simulations, IEEE J. Sel. Topics Appl. Earth Obs., 10(11) (2017).

HOW TO CITE THIS ARTICLE

N. Radkani, B. Zakeri, Sea Surfaces Scattering by Multi-Order Small-Slope Approximation: A Monte-Carlo and Analytical Comparison, AUT J. Elec. Eng., 51(2) (2019) 123-130.

DOI: 10.22060/eej.2019.14446.5229